# Compact Microstrip 3-dB Coupled-Line Ring and Branch-Line Hybrids With New Symmetric Equivalent Circuits

Hee-Ran Ahn, *Senior Member, IEEE*, and Sangwook Nam, *Senior Member, IEEE*

***Abstract*—New symmetric equivalent circuits are suggested for 90° and 270° transmission-line sections, with which compact coupled-line ring and branch-line hybrids can be designed and fabricated. For this purpose, firstly stepped-impedance transmission-line (SITL) sections, being equivalent to a uniform transmission-line section with arbitrary electrical lengths, are synthesized, and design formulas for the SITL sections are derived. Secondly, three types of equivalent circuits are introduced by combining the SITL sections with coupled-line Π-, modified Π-, or $T$-type, and are called stepped-impedance coupled-line Π-type (SCΠ), stepped-impedance modified $T$-type (SMT), and stepped-impedance modified Π-type (SMΠ). The SCΠs are for 270° transmission-line sections, while both SMTs and SMΠs are for 90° transmission-line sections. Based on the suggested equivalent circuits, compact coupled-line ring and branch-line hybrids designed at 1 GHz are fabricated, and the measured bandwidth of the ring hybrid is 50% with 15-dB return loss. The measured results may be considered as excellent, reflecting their total transmission-line lengths of 183° and 111° for the ring and branch-line hybrids, respectively.**

***Index Terms*—Asymmetric structures, compact branch-line hybrids, compact coupled-line ring hybrids, compact equivalent circuits, compact rat-race couplers, stepped-impedance coupled-line Π-types (SCΠs), stepped-impedance modified Π-types (SMΠs), stepped-impedance modified $T$-types (SMTs), symmetric equivalent circuits.**

## I. INTRODUCTION

THE RING and branch-line hybrids [1]–[3] are key components for microwave applications, such as balance mixers, balanced amplifiers, and antenna arrays. As the wireless communication systems require substantial reduction in mass and volume, compactness of such hybrids becomes of high interest [4]. The ring and branch-line hybrids consist of 90° or 270° transmission-line sections, which should be reduced for the compactness, and the reduction methods depend on which equivalent circuits of those transmission-line sections are employed [5]–[46]. The employed equivalent circuits are generally classified into symmetric and asymmetric structures, but the asymmetric structures [8]–[11], [40] seem to not be suitable to be replaced with 90° transmission-line sections without any modification, which will be clarified later with one of asymmetric structures [12]–[15], constant voltage standing-wave ratio type transmission-line impedance transformers (CVTs) [12].

The symmetric equivalent circuits are lumped-element models [3], [16]–[20], [38], [46], Π-type [5], [21]–[26], $T$-type [25]–[27], [34], modified Π- [28], [41] and $T$-types [28], [29], dual transmission-line sections [39], [42] and stepped-impedance transmission-line (SITL) sections [30], [31], where the equivalent circuits requiring series capacitances or inductances are classified into the lumped-element models. The Π- and $T$-types may be the same as the modified Π- and $T$-types with $N = 1$ [28]. The artificial transmission-line model in [29] looks very similar to the modified $T$-equivalent circuit, but the design formulas seem to be approximation expression and optimization is therefore required for desired performance. For the dual transmission-line sections [39], [42], since two transmission-line sections are of different lengths [39], meandering is indispensable, which results in inflexible fabrication. In [30] and [31], the investigation on the SITL sections is carried out, but valid for only 90°[30] and 60°[31] transmission-line sections.

Using the Π-, $T$-type or SITL sections, the ring and branch-line hybrids may be reduced, but the performance of the resulting hybrids is worse than that of the original ones if the electrical length of a transmission-line section is reduced from 90° to 50° (more or less), and so do those with lumped element models [3]. In addition to the worse performance, the ring hybrids reduced by the conventional methods do not appear to be significantly compact [10], [11], [21]–[23], [26], [27], [29]–[32], [35]–[38] because three 90° equivalent circuits are substituted for a 270° transmission-line section of the ring hybrids. On the contrary, there is only one case of the compact ring hybrids [5] that a 270° equivalent circuit is directly replaced with the 270° transmission-line section, but they should be implemented with 3-D structures [5].

In this paper, to overcome the conventional problems, design formulas for the SITL sections are derived for a uniform transmission-line section with arbitrary electrical lengths, and new symmetric equivalent circuits for 90° or 270° uniform transmission-line sections are suggested for more design flexibility, easier implementation with 2-D structures, and better frequency

Manuscript received September 06, 2012; revised January 02, 2013 and January 08, 2013; accepted January 10, 2013. Date of publication February 07, 2013; date of current version March 07, 2013. This work was supported by the Korea Government [Ministry of Education, Science and Technology (MEST)] under National Research Foundation of Korea (NRF) Grant 2011-0001270.

The authors are with the INMC, School of Electrical Engineering and Computer Science, Seoul National University, Seoul 151-742, Korea (e-mail: hranahn@gmail.com; snam@snu.ac.kr).

Color versions of one or more of the figures in this paper are available online at http://ieeexplore.ieee.org.

Digital Object Identifier 10.1109/TMTT.2013.2241783

TABLE I
COMPARISONS BETWEEN CONVENTIONAL AND PROPOSED BRANCH-LINE HYBRIDS

| Refs. | Transmission-line lengths | Power divisions (dB) | Equivalent circuits |
|---|---|---|---|
| [11] | 40.0° x 47.7° | -3.36, -3.25 | Asymmetric |
| [17] | 39.6° x 43.2° | - | Lumped |
| [43] | 44.7° x 40.4° | -3.9±0.1 | Quasi-Π |
| [44] | 43.2° x 50.4° | better than -4.0 | Π-type |
| [46] | 45.0° x 45.0° | -4.00, -4.00 | Π-type |
| This work | 24.2° x 31.4° | -3.02, -3.48 | Proposed SMΠ |

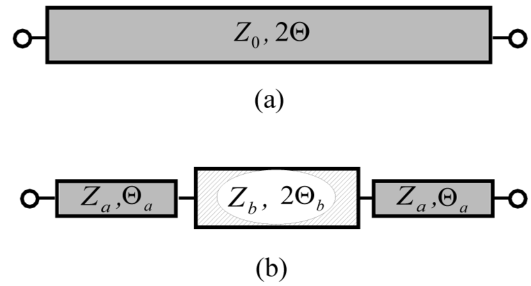

Fig. 1. Transmission-line sections. (a) Uniform transmission-line section. (b) SITL sections.

performance. The equivalent circuits may be obtained by combining the SITL sections with coupled-line Π-type [5], modified Π-, or $T$-type [28] and named stepped-impedance coupled-line Π-type (SCΠ), stepped-impedance modified $T$-type (SMT), and stepped-impedance modified Π-type (SMΠ). The SCΠs are for the 270° uniform transmission-line sections, while both SMTs and SCΠs are for the 90° transmission-line sections. The three equivalent circuits proposed in this paper each have two identical transmission-line sections at both ends, with which more design flexibility and easier implementation can be possible.

To claim additional advantages of the suggested equivalent circuits, it will be demonstrated later that the frequency performance of the SMTs and SMΠs can be the same as that of the 90° transmission-line sections, even with the total lengths reduced. It will also be illustrated that the frequency response of the SMΠ is, in the frequency range of interest, better than the conventional Π-type, even though the SMΠ is much shorter than one-third of the conventional one. Since the two points mentioned above are the properties that have never been verified before with the conventional equivalent circuits [5]–[27], [29]–[46], the suggested equivalent circuits may have a big advantage over the conventional methods.

Based on the new equivalent circuits, the coupled-line ring and branch-line hybrids are fabricated at a design center frequency of 1 GHz and the measured results agree with those predicted. The transmission-line sections are directly related with the size reduction, and total lengths of the ring and branch-line hybrids implemented in this paper are 183° and 111°, respectively.

The implemented coupled-line ring hybrid may be compared with only one with the total length of 220° [5] and considered to be better, in terms of size reduction and easier realization with microstrip formats. The fabricated branch-line hybrid is compared with the conventional ones in Table I where the size of the branch-line hybrid [43] is not exactly specified and therefore approximated by physical dimensions, substrate, and center frequency given. The data in Table I inform that the suggested branch-line hybrid is the best in the perspective of compactness and frequency performance.

In this paper, unsuitability of asymmetric structures for ring and branch-line hybrids will be explained first, then design formulas of new symmetric equivalent circuits will be derived. Based on the derived equivalent circuits, coupled-line ring and branch-line hybrids will be designed and fabricated. For the better understanding of three equivalent circuits called SCΠ, SMT, and SMΠ, additional explanations will be added. The first letter S indicates the SITL sections (Fig. 1), while the center letter C is related with the coupled transmission-line sections [5], and that of M is from the modified equivalent circuits [28]. The last letters of Π or T are associated with the locations of the open stubs [5], [28].

## II. UNSUITABILITY OF ASYMMETRIC STRUCTURES

Asymmetric structures [8]–[11], [40] have been replaced with 90° transmission-line sections to reduce the size of the ring and branch-line hybrids, but they are not suitable for this purpose. The reasons for the inappropriateness will be clarified. To discuss them, SITL sections, being equivalent to a uniform transmission-line section with arbitrary electrical lengths, should be discussed.

Two transmission-line sections are depicted in Fig. 1 where a uniform transmission-line section is in Fig. 1(a) and the SITL sections are in Fig. 1(b). The uniform transmission-line section is $2\Theta$ long and has the characteristic impedance of $Z_0$, while the SITL sections consist of three transmission-line sections, two of which located at both ends are each $\Theta_a$ long and have identical characteristic impedance of $Z_a$, and one of which is $2\Theta_b$ long and has $Z_b$ characteristic impedance. To synthesize one of the asymmetric structures (CVTs) [12], the equivalent circuit in Fig. 1(b) needs to be studied.

### A. SITL Sections

The even- and odd-mode impedances ($Z_{\rm ev}$ and $Z_{\rm od}$) of the uniform transmission-line section in Fig. 1(a) are

$$Z_{\rm ev} = -jZ_0 \cot\Theta \tag{1a}$$

$$Z_{\rm od} = jZ_0 \tan\Theta. \tag{1b}$$

Those ($Z_{{\rm ev}\_SI}$ and $Z_{{\rm od}\_SI}$) of the SITL sections in Fig. 1(b) are

$$Z_{{\rm ev}\_SI} = -jZ_a \frac{Z_b \cot\Theta_b - Z_a \tan\Theta_a}{Z_a + Z_b \cot\Theta_b \tan\Theta_a} \tag{2a}$$

$$Z_{{\rm od}\_SI} = jZ_a \frac{Z_b \tan\Theta_b + Z_a \tan\Theta_a}{Z_a - Z_b \tan\Theta_b \tan\Theta_a}. \tag{2b}$$

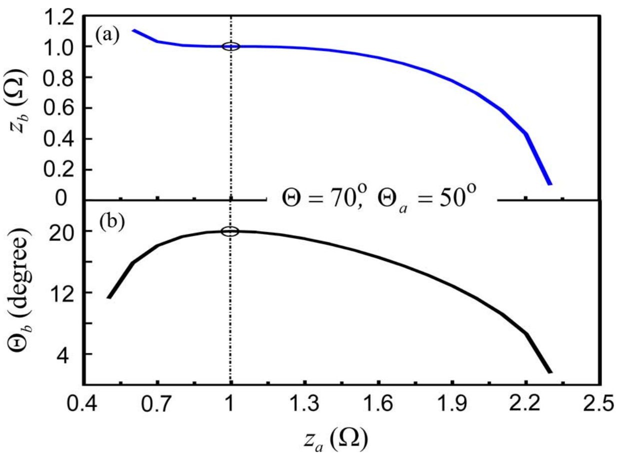


Fig. 2. Calculation results versus $z_a$. (a) $z_b$. (b) $\Theta_b$.

Design formulas for $Z_b$ and $\Theta_b$ in Fig. 1(b) are derived by equating two sets of equations in (1) and (2) to give

$$z_b = z_a \sqrt{\left(\frac{\cot\Theta + z_a \tan\Theta_a}{z_a - \cot\Theta \cdot \tan\Theta_a}\right)\left(\frac{\tan\Theta - z_a \tan\Theta_a}{z_a + \tan\Theta \cdot \tan\Theta_a}\right)} \tag{3a}$$

$$\tan\Theta_b = \sqrt{\left(\frac{z_a - \cot\Theta \cdot \tan\Theta_a}{z_a + \tan\Theta \cdot \tan\Theta_a}\right)\left(\frac{\tan\Theta - z_a \tan\Theta_a}{\cot\Theta + z_a \tan\Theta_a}\right)} \tag{3b}$$

where $z_a = Z_a/Z_0$, $z_b = Z_b/Z_0$, $\Theta < 90^\circ$ ($\Theta \neq 90^\circ$), and $\Theta \geq \Theta_a + \Theta_b$. The values of $z_b$ and $\Theta_b$ are determined by arbitrary values of $z_a$ and $\Theta_a$. To have real values of $z_b$ and $\Theta_b$ in (3), the following conditions in (4) should be satisfied for $z_a$.

For $T_1 > T_2$,

$$T_2 < z_a < T_1 \tag{4a}$$

and for $T_1 \leq T_2$,

$$T_1 \leq z_a \leq T_2 \tag{4b}$$

where $T_1 = \tan\Theta \cdot \cot\Theta_a$ and $T_2 = \cot\Theta \cdot \tan\Theta_a$.

Based on the design formulas derived in (3) and (4), the characteristic impedances of $z_b$ and the electrical lengths of $\Theta_b$ were calculated by varying $z_a$. If $\Theta = 70^\circ$ and $\Theta_a = 50^\circ$ are chosen, $T_1 > T_2$ due to $T_1 = 2.3$ and $T_2 = 0.43$ in (4). Therefore, $z_a$ should be from 0.43 to 2.3 from the valid equation in (4a).

The calculation results are plotted in Fig. 2 and listed in Table II. When $z_a = 1$, $z_b = 1$ and $\Theta_b = 20^\circ$ are obtained as listed in Table II and Fig. 2. It means that if $Z_a = Z_0$ is chosen in Fig. 1(b), $Z_b$ becomes the same as $Z_a$, and the resulting SITL sections become the uniform transmission-line section with no difference between $Z_a$ and $Z_b$. When $z_a < 1$ in Fig. 2 and Table II, the values of $z_b$ become greater than unity, and the electrical lengths of $\Theta_b$ are less than 20°. When $z_a > 1$, those of $z_b$ and $\Theta_b$ decrease gradually. Five SITL sections

TABLE II
DESIGN VALUES FOR $z_b$ AND $\Theta_b$ DEPENDING ON $z_a$ WITH $\Theta = 70^\circ$ AND $\Theta = 50^\circ$ FIXED

| Θ = 70° and Θ$_a$ = 50° | | |
|---|---|---|
| $z_a = \dfrac{Z_a}{Z_0}$ | $z_b = \dfrac{Z_b}{Z_0}$ | $\Theta_b$ (°) |
| 0.5 | 1.4370 | 11.219 |
| 1.0 | 1.0 | 20.000 |
| 1.5 | 0.9554 | 17.518 |
| 2.0 | 0.6958 | 11.219 |
| 2.3 | 0.1009 | 1.5100 |

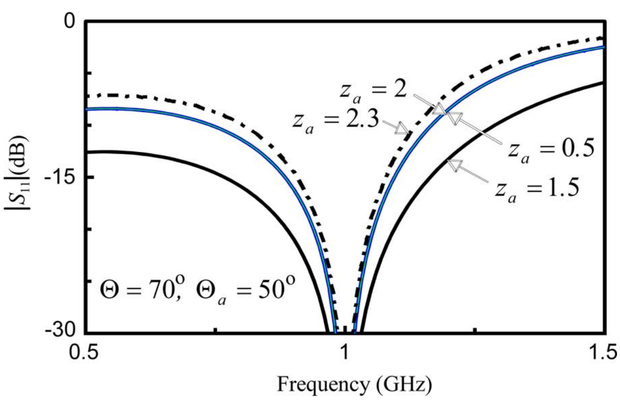


Fig. 3. Frequency responses with various $z_a$.

in Table II were simulated and the frequency responses are displayed in Fig. 3 where the bandwidth with $z_a = 1.5$ is the widest, while that with $z_a = 2.3$ is the smallest, and the two cases with $z_a = 2$ and $z_a = 0.5$ have the same performance. From the frequency responses in Fig. 3, one can know that the bandwidths of SITL sections are proportional to the total lengths of $\Theta_a + \Theta_b$. When $z_a = z_b = 1$, i.e., the SITL sections are the same as the uniform transmission-line section, the SITL sections are the longest with $\Theta_a + \Theta_b = \Theta$ and therefore it is natural that its bandwidth is wider than any other in Table II and Fig. 2.

### B. CVTs as Impedance Transformers

Halves of the transmission-line sections in Fig. 1(a) and (b) are described in Fig. 4 where half of the SITL sections in Fig. 4(b) is the CVT [12]. The asymmetric $T$-structure in [11] and modified CVT (MCVT) in [14] are additionally illustrated in Fig. 4(c) and (d). Even though the SITL sections in Fig. 1(b) are equivalent to a uniform transmission-line section in Fig. 1(a), the CVT in Fig. 4(b) cannot be equivalent to a transmission-line section with the characteristic impedance of $Z_0$ and the electrical length of $\Theta$, which is very important point and will be clarified in more detail. For this, input impedances at port ② with port ① terminated in $Z_0$ are indicated as $Z_{in\_0}$ and $Z_{\text{in\_CVT}}$ in Fig. 4(a) and (b). In this case, $Z_{in\_0}$ is always $Z_0$ in any case, but $Z_{\text{in\_CVT}}$ cannot be $Z_0$, except one case with $Z_a = Z_b$. The input impedance of $Z_{\text{in\_CVT}}$ is expressed as

$$Z_{\text{in\_CVT}} = Z_b \frac{Z_a \frac{Z_0 + jZ_a \tan\Theta_a}{Z_a + jZ_0 \tan\Theta_a} + jZ_b \tan\Theta_b}{Z_b + j\left(Z_a \frac{Z_0 + jZ_a \tan\Theta_a}{Z_a + jZ_0 \tan\Theta_a}\right)\tan\Theta_b}. \tag{5}$$

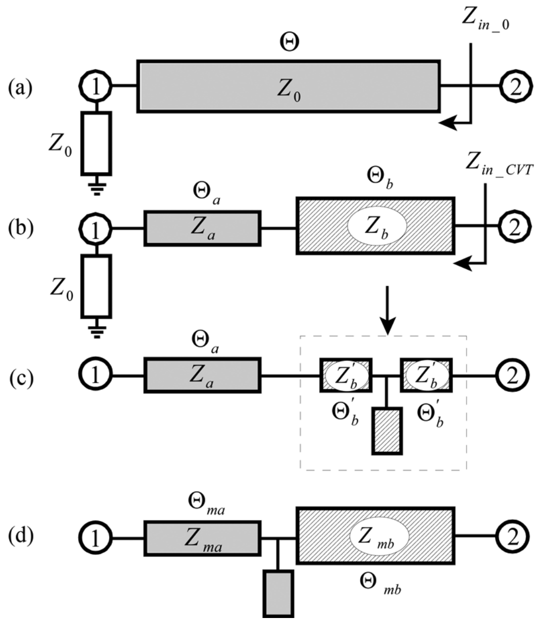


Fig. 4. Various circuits. (a) Uniform transmission-line section. (b) CVT. (c) Asymmetric $T$-structure if $Z_b' = Z_a$. (d) MCVT [14].

The input impedance of $Z_{\mathrm{in\_CVT}}$ normalized to $Z_0$, $z_{\mathrm{in\_CVT}}$, is simplified as

$$z_{\mathrm{in\_CVT}} = z_b \frac{p + jq}{r + js} \tag{6}$$

where $z_b = Z_b/Z_0$ and

$$p = z_a - z_b \tan\Theta_a \tan\Theta_b \tag{6a}$$
$$q = z_a^2 \tan\Theta_a + z_a z_b \tan\Theta_b \tag{6b}$$
$$r = z_a z_b - z_a^2 \tan\Theta_a \tan\Theta_b \tag{6c}$$
$$s = z_a \tan\Theta_b + z_b \tan\Theta_a. \tag{6d}$$

To have real value of $z_{\mathrm{in\_CVT}}$, the following relation holds:

$$ps - qr = 0. \tag{7}$$

Substituting (7) into $z_{\mathrm{in\_CVT}}$ in (6) results in

$$z_{\mathrm{in\_CVT}} = z_b \frac{q}{s} = z_a z_b \frac{z_a \tan\Theta_a + z_b \tan\Theta_b}{z_a \tan\Theta_b + z_b \tan\Theta_a} = IR \tag{8}$$

where $IR$ is an impedance transformation ratio to transform $Z_0$ into $Z_{\mathrm{in\_CVT}}$ in Fig. 4(b).

If $z_a = z_b$ in (8), $z_b$ and $z_a$ have unit values as listed in Table II, and therefore, $IR$ becomes unity. Otherwise, the CVT is an impedance transformer to transform unit value of impedance into $IR$, where $IR \neq 1$. Therefore, the assumption that the CVT can be terminated in equal impedance of $Z_0$[11, Fig. 1] seems to be incorrect. When $Z_b < Z_a$ in Fig. 4(b), the transmission-line section with $Z_b$ may be converted to a $T$-equivalent circuit having two identical transmission-line sections with the characteristic impedance of $Z_b'$ and the electrical length of $\Theta_b'$ and an open stub as described in Fig. 4(c). If $Z_b'$ is the same as $Z_a$, the structure in Fig. 4(c) is the same as the asymmetric $T$-structure suggested in [11]. The structure in Fig. 4(d) looks similar to the asymmetric $T$-structure in [8]–[11], and [40], but if the characteristic impedances of $Z_{ma}$ and $Z_{mb}$ are different, it is a MCVT [14], which may be interpreted with a different way. The CVTs may be designed by the methods in [12] and [14], and the data for the CVTs with $IR = 2$ are given in Table III where the termination impedance of $Z_0$ in Fig. 4(b) is assumed 50 Ω, and effective electrical lengths of $\Theta_{\mathrm{eff}}$ are computed from a scattering parameter of $S_{21}$[47]–[49] such as

TABLE III
DESIGN DATA FOR CVTs WITH $IR = 2$

| $Z_a(\Omega)$ | $\Theta_a$ | $Z_b(\Omega)$ | $\Theta_b$ | $\Theta_{eff}$ |
|---|---|---|---|---|
| 72.45 | 68.73° | 50 | 10° | 80.0° |
| 75.03 | 57.97° | 50 | 15° | 74.6° |
| 79.70 | 47.02° | 50 | 20° | 70.0° |
| 88.80 | 35.65° | 50 | 25° | 65.0° |

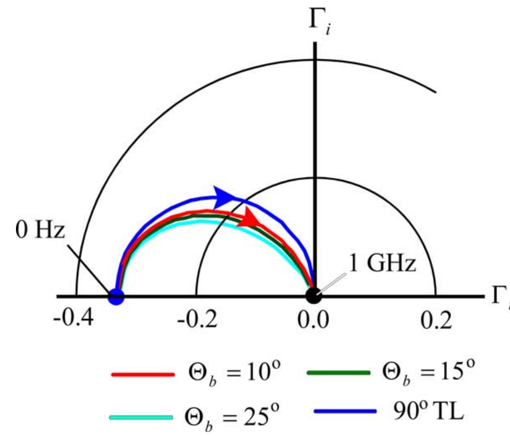


Fig. 5. Simulated scattering parameters of $S_{22}$.

$$\Theta_{\mathrm{eff}} = -\angle S_{21} = \tan^{-1}\left(\frac{B + C \cdot IR}{A \cdot IR + D}\right) \tag{9}$$

where

$$A = \cos\Theta_a \cos\Theta_b - \frac{z_a}{z_b} \sin\Theta_a \sin\Theta_b \tag{9a}$$
$$B = z_a \sin\Theta_a \cos\Theta_b + z_b \cos\Theta_a \sin\Theta_b \tag{9b}$$
$$C = \frac{1}{z_a} \sin\Theta_a \cos\Theta_b + \frac{1}{z_b} \cos\Theta_a \sin\Theta_b \tag{9c}$$
$$D = \cos\Theta_a \cos\Theta_b - \frac{z_b}{z_a} \sin\Theta_a \sin\Theta_b. \tag{9d}$$

Based on the data in Table III, the scattering parameters of $S_{22}$ of the CVTs in Fig. 4(b) were simulated from 0 to 1 GHz with the center frequency of 1 GHz, where port ② is placed close to the transmission-line section with $Z_b$, as depicted in Fig. 4(b). The simulated results are plotted in polar coordinates in Fig. 5 where the different CVTs are expressed as the lengths of $\Theta_b$ and "90° TL" is a quarter-wave impedance transformer to transform 50 into 100 Ω with the characteristic impedance of 70.71 Ω. In this case, the scattering parameter of $S_{22}$ is expressed as

$$S_{22} = \frac{z_{\mathrm{in\_CVT}} - IR}{z_{\mathrm{in\_CVT}} + IR}. \tag{10}$$

When the operating frequency of $f$ is 0 GHz, $z_{\mathrm{in\_CVT}}$ in Fig. 4(b) is unity, and therefore, $S_{22} = -0.333$ with $IR = 2$.

When $f = 1$ GHz, all are perfectly matched, and therefore, $S_{22} = 0$. Taking a close look at the changes between 0 and 1 GHz in Fig. 5, the magnitudes of $S_{22}$ of the CVT with $\Theta_b = 25°$ are the smallest, which means that smallest length is required to match 50 to 100 Ω. As listed in Table III, the effective electrical length of $\Theta_{\text{eff}}$ with $\Theta = 25°$ is the smallest, while that with $\Theta = 10°$ is the longest, but the phase delay of the CVTs with $IR = 2$ cannot be 90°. That is, the CVTs can be impedance transformers, but cannot be the same as 90° impedance transformers due to different phase angles.

### C. Summary

The reasons why the asymmetric structures of CVTs cannot be replaced with any 90° transmission-line section were explained above. To sum up, the SITL sections themselves in Fig. 1(b), from which the CVTs are derived, cannot be defined at 90° in (3b), which is the first reason. The input impedances of $Z_{\text{in\_CVT}}$ in Fig. 4(b) cannot be $Z_0$ as far as $Z_a \neq Z_b$, which is the second reason. The 90° transmission-line sections of the ring and branch-line hybrids are impedance transformers and have 90° phase angle. However, the CVTs in Table III can be impedance transformers to convert unit impedance into $IR = 2$, but the phase angles are not 90°, which is the third reason.

Due to the fundamental reasons explained above, only symmetric structures can be substituted for 90° and 270° transmission-line sections of the ring and branch-line hybrids. Thus, the new symmetric equivalent circuits will be discussed, and ways to miniaturize their circuit size will be evolved.

## III. Symmetric Equivalent Circuits

To reduce the size of ring and branch-line hybrids, 90° or 270° transmission-line sections need to be made smaller. For this, new equivalent circuits may be obtained by combining the SITL sections and conventional ones [5], [28]. Three types of equivalent circuits are depicted in Fig. 6 where the one in Fig. 6(a) is for the 270° transmission-line section with the characteristic impedance of $Z_0$, while the two others in Fig. 6(b) and (c) are for 90° ones with $Z_0$. The one in Fig. 6(a) is called SCΠ and the two others are differentiated as SMT and SMΠ.

The SCΠ in Fig. 6(a) consists of one set of coupled transmission-line sections with two short circuits in a diagonal direction and pairs of open stubs and transmission-line sections. The coupled transmission-line sections, of which the even- and odd-mode impedances are $Z_{0e}$ and $Z_{0o}$, are $\Theta_{sC}$ long. The characteristic impedances of the transmission-line section and open stub are $Z_a$ and $Z_{oC}$ and the electrical lengths are $\Theta_a$ and $\Theta_{oC}$, as described in Fig. 6(a). With the transmission-line sections with $Z_a$ and $\Theta_a$ in Fig. 6(a), it is easier to fabricate the coupled transmission-line sections with 2-D structures. It is also easier to connect the coupled transmission-line sections to other transmission-line sections or ports because the two points, where two open stubs are connected to the coupled transmission-line sections, are not placed in a straight line. To solve this problem, the two transmission-line sections with $Z_a$ and $\Theta_a$ are needed and may be determined arbitrarily depending on design situation.

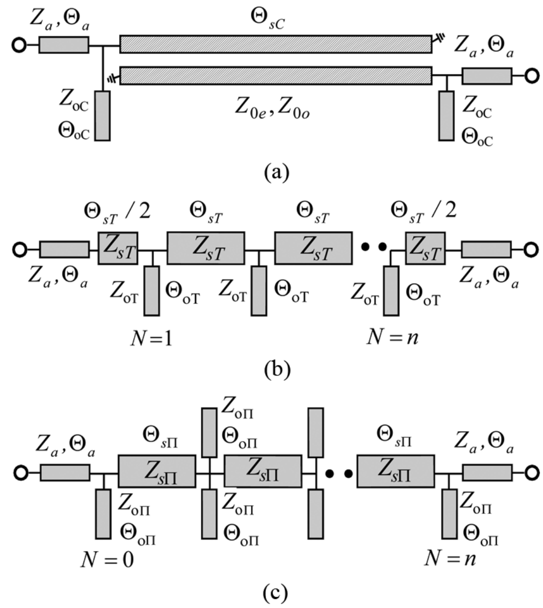


Fig. 6. 270° or 90° equivalent circuits with the characteristic impedance of $Z_0$. (a) SCΠ for 270° transmission-line section. (b) SMT for 90° transmission-line section. (c) SMΠ for 90° transmission-line section.

The SMT or SMΠ in Fig. 6(b) and (c) can be considered from the SITL sections with three transmission-line sections in Fig. 1(b). Among the SITL sections in Fig. 1(b), leaving the two transmission-line sections with $Z_a$ and $\Theta_a$ unchanged and converting the one transmission-line section with $Z_b$ and $2\Theta_b$ to the modified $T$- or Π-equivalent circuit [28], the SMT or SMΠ is obtained.

The SMT consists of two identical transmission-line sections with $Z_a$ and $\Theta_a$ and a modified $T$-equivalent circuit. The modified $T$-equivalent circuit is composed of $N$ open stubs and $N+1$ transmission-line sections. The electrical length of the first and last transmission-line sections with the characteristic impedance of $Z_{sT}$ is $\Theta_{sT}/2$ and the others are therefore two times of the first or last one. The open stub with the characteristic impedance of $Z_{oT}$ is $\Theta_{oT}$ long.

SMΠ also includes two identical transmission-line sections with $Z_a$ and $\Theta_a$ and a modified Π-equivalent circuit. The modified Π-equivalent circuit has $N$ transmission-line sections with the characteristic impedance of $Z_{s\Pi}$ and $N+1$ open stubs. The transmission-line sections and the open stubs are equally $\Theta_{s\Pi}$ and $\Theta_{o\Pi}$ long, respectively, and the characteristic impedance of the open stub is $Z_{o\Pi}$. The transmission-line section with the characteristic impedance of $Z_a$ and the electric length of $\Theta_a$ is necessary for easier fabrication and more design flexibility and may be determined arbitrarily depending on design situations.

The design formulas for the three types of SCΠ, SMT, and SMΠ are

$$Z_{0e} = Z_2 \frac{\sin\Theta_2}{\sin\Theta_{sC}} \frac{C}{1-C} \tag{11a}$$

$$Z_{0o} = Z_2 \frac{\sin\Theta_2}{\sin\Theta_{sC}} \frac{C}{1+C} \tag{11b}$$

$$\begin{aligned} S_C &= Y_{oC} \cdot \tan\Theta_{oC} \\ &= \frac{1}{C \cdot Z_2} \left( \frac{\cos\Theta_{sC} - C \cdot \cos\Theta_2}{\sin\Theta_2} \right) \end{aligned} \tag{11c}$$

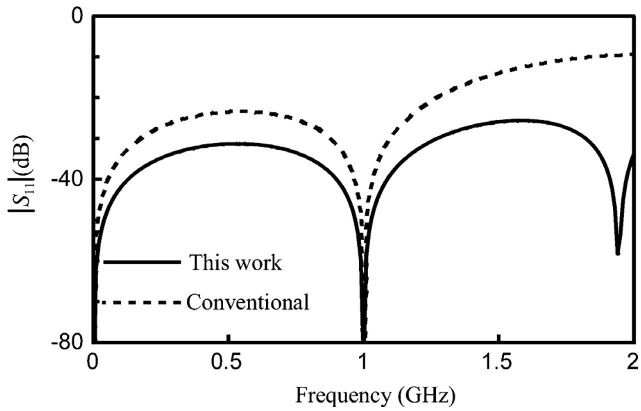


Fig. 7. Compared frequency responses between one SCΠ and one conventional equivalent circuit [25].

$$Z_{sT} = Z_2 \frac{\tan \frac{\Theta_2}{2N}}{\tan \frac{\Theta_{sT}}{2}} \tag{12a}$$

$$\begin{aligned} S_T &= Y_{oT} \cdot \tan \Theta_{oT} \\ &= \frac{2}{Z_{sT}} \cdot \frac{Z_{sT} - Z_2 \cot \frac{\Theta_2}{2N} \tan \frac{\Theta_{ST}}{2}}{Z_{sT}\ \tan \frac{\Theta_{sT}}{2} + Z_2 \cot \frac{\Theta_2}{2N}} \end{aligned} \tag{12b}$$

$$Z_{s\Pi} = Z_2 \frac{\sin \frac{\Theta_2}{N}}{\sin \Theta_{s\Pi}} \tag{13a}$$

$$S_\Pi = Y_{o\Pi} \cdot \tan \Theta_{o\Pi} = \frac{1}{Z_2} \left( \frac{\cos \Theta_{s\Pi} - \cos \frac{\Theta_2}{N}}{\sin \frac{\Theta_2}{N}} \right) \tag{13b}$$

where $N$ is a positive integer including 0, $S_C$, $S_T$, and $S_\Pi$ are susceptances generated by each open stub, $C$ is a coupling coefficient, and $Z_2$ and $\Theta_2$ are obtained by substituting $\Theta = 45^\circ$ in Fig. 1(b), giving

$$Z_2 = Z_a \sqrt{\frac{Z_a^2 \tan^2 \Theta_a - Z_0^2}{Z_0^2 tan^2 \Theta_a - {Z_a}^2}} \tag{14a}$$

$$\Theta_2 = 2 \left( \tan^{-1} \sqrt{\frac{(Z_0 - Z_a \tan \Theta_a)(Z_a - Z_0 \tan \Theta_a)}{(Z_0 + Z_a \tan \Theta_a)(Z_a + Z_0 \tan \Theta_a)}} \right) \tag{14b}$$

where, if $\Theta_a = 0^\circ$, $\Theta_2$ becomes $90^\circ$.

If $\Theta_a = 0^\circ$, the SCΠ in Fig. 6(a) is the same as the coupled-line Π-type in [5], and the SMT and SMΠ in Fig. 6(b) and (c) are the modified Π- and $T$-types [28]. With $\Theta_a = 0^\circ$ and $N = 1$, the SMT and SMΠ are conventional $T$-type [26], [27], [34] and Π-type [21]–[26], [33], [36], [44]. With $\Theta_a = 0^\circ$ and $N = 2$ in Fig. 6(c), SMΠ is the same as the combination model in [25].

For a 90° transmission-line section with the characteristic impedance of 35.35 Ω, the design data of SMΠ with $\Theta_a = 0^\circ$, $N = 2$, and $\Theta_{s\Pi} = 30^\circ$ are computed as $Z_{s\Pi} = 49.9924\ \Omega$ and $S_\Pi = 157.289^{-1}$ ℧ based on (13). The susceptance of $S_\Pi$ may be equal to the capacitance value of 1.012 pF at 1 GHz. On the other hand, based on those in [25, eqs. (9)–(11)] of the combination model, $Z_{s\Pi} = 46.4295\ \Omega$ and $S_{\Pi e} = S_{\Pi c} = 110.909^{-1}$ ℧ are calculated, where $S_{\Pi e}$ and $S_{\Pi c}$ are the susceptances generated by the open stubs located at both ends and the center of the combination-model in [25, Fig. 12], respectively, and equal to 1.435 pF at 1 GHz. The two cases were simulated at the design center frequency of 1 GHz, and the frequency responses are compared in Fig. 7 where the solid and dotted lines are those of the SMΠ and the combination-model [25], respectively. As can be seen, the designed SMΠ is perfectly matched at 1 GHz and shows better frequency performance than that of the combination model in whole frequencies of interest.

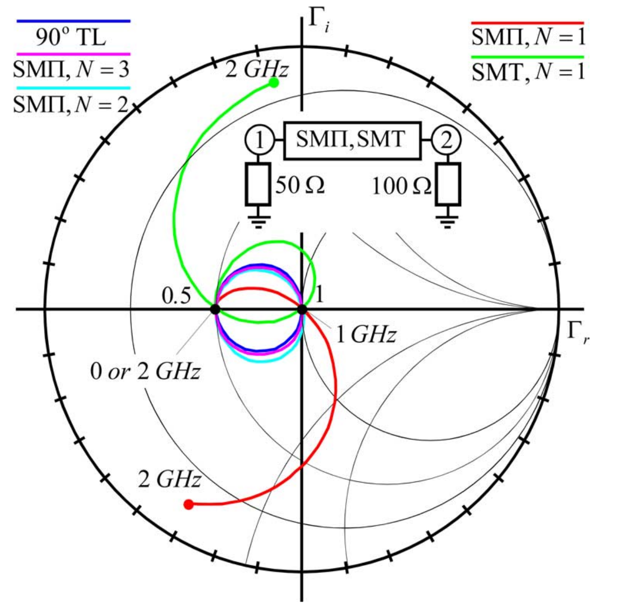


Fig. 8. Scattering parameters of $S_{22}$ on an impedance Smith chart normalized to 100 Ω.

Letting $\Theta_a = 0^\circ$ and fixing $N\Theta_{sT} = N\Theta_{s\Pi} = 50^\circ$ in Fig. 6(b) and (c), several SMΠs and one SMT to transform 50 into 100 Ω are designed and the design data are in Table IV where the susceptances of $S_\Pi$ and $S_T$ are expressed with the capacitance of $C_{ap}$ at 1 GHz. The SMΠs and one SMT were simulated for the scattering parameters of $S_{22}$ at 100 Ω termination impedance, and the simulation results are illustrated on a Smith chart normalized to 100 Ω (see Fig. 8) where the operating frequencies are from 0 to 2 GHz with the center frequency of 1 GHz. The quarter-wave impedance transformer expressed as "90° TL" in Fig. 8 draws a circle cutting two points of 50 Ω (0.5) and 100 Ω (1). The SMΠ with $N = 3$ also draws a circle, which is very similar to that of "90° TL." The SMΠ with $N = 2$ makes a circle, but slightly deviates from the circle with "90° TL." However, the trajectories of the SMΠ with $N = 1$ or SMT with $N = 1$ do not form any circle and diverge from the circle. In this case, SMΠ and SMT with $N = 1$ are the conventional Π- and $T$-types. From the results of the scattering parameters of $S_{22}$, it can be concluded that the number of $N$'s should be greater than or equal to 2 for the desired performance.

Using the new equivalent circuits suggested in this paper, compact ring and branch-line hybrids will be designed.

## IV. Compact Coupled-Line Ring Hybrids

### A. Coupled-Line Ring Hybrids

Since the ring hybrid consists of three 90° and one 270° transmission-line sections with the characteristic impedance of 70.71 Ω, a 270° transmission-line section will be synthesized

TABLE IV
DESIGN DATA OF SMΠS AND SMT WITH FIXING $\Theta_a = 0°$ AND $N\Theta_{s\Pi} = N\Theta_{sT} = 50°$ TO TRANSFORM 50 INTO 100 Ω

| Type | $N$ | $Z_{s\Pi}(\Omega)$ | $S_{\Pi}^{-1}(\Omega)$ | $C_{ap}$ [pF] |
|---|---|---|---|---|
| SMΠ | $N = 4$ | 125.021 | 516.241 | 0.3083 |
| SMΠ | $N = 3$ | 123.273 | 384.443 | 0.4140 |
| SMΠ | $N = 2$ | 118.309 | 251.000 | 0.6341 |
| SMΠ | $N = 1$ | 92.305 | 110.005 | 1.4468 |
| | | $Z_{sT}(\Omega)$ | $S_T^{-1}(\Omega)$ | $C_{ap}$ [pF] |
| SMT | $N = 1$ | 151.638 | 90.3576 | 1.7614 |

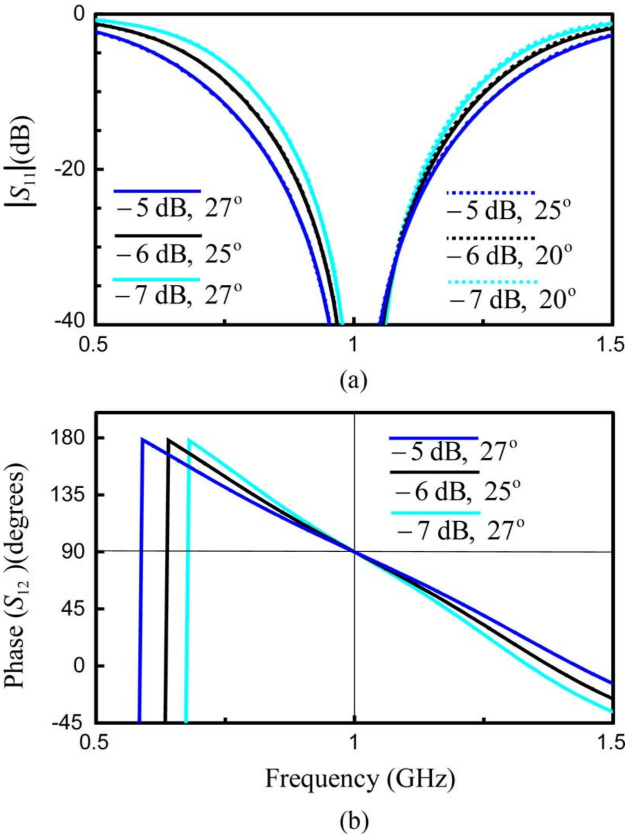


Fig. 9. Frequency responses of SCΠs. (a) Matching of $|S_{11}|$. (b) Phases of $S_{12}$.

first. If $Z_a = 120\ \Omega$ and $\Theta_a = 5°$ in Fig. 6(a) are chosen, $Z_2 = 70.02\ \Omega$ and $\Theta_2 = 78.55°$ are calculated based on the equations in (14).

Varying $\Theta_{sC}$ and coupling coefficients of $C$ in Fig. 6(a), the even- and odd-mode impedances of $Z_{0e}$ and $Z_{0o}$ and the susceptances of $S_C$ are calculated in Table V where $Z_{0e}$ and $Z_{0o}$ increase with the coupling coefficients, but decrease with lengths of $\Theta_{sC}$. Six cases among those in Table V were simulated and the frequency responses are plotted in Fig. 9 where matching and phase responses are in Fig. 9(a) and (b). If the coupling coefficient is the same in Fig. 9(a), almost identical responses are shown, independently of the electrical lengths of $\Theta_{sC}$, and the bandwidths are proportional to the coupling coefficients. All the designed 270° transmission-line sections show 270° phase angle in Fig. 9(b) (refer to $\Theta_{\text{eff}} = -\angle S_{21}$), which indicates that the 270° transmission-line section can be realized with the transmission-line sections less than 37° long.

TABLE V
DESIGN EXAMPLES OF SCΠS WITH $Z_a = 120\ \Omega$ AND $\Theta_a = 5°$ FIXED

| $\Theta_{sC}$(°) \ $C$(dB) | | -5 | -6 | -7 | -8 |
|---|---|---|---|---|---|
| 27 | $Z_{0e}(\Omega)$ | 194.2 | 151.9 | 122.0 | 99.98 |
| | $Z_{0o}(\Omega)$ | 54.40 | 50.47 | 46.67 | 43.04 |
| | $S_C^{-1}(\Omega)$ | 49.52 | 43.45 | 38.21 | 33.65 |
| 25 | $Z_{0e}(\Omega)$ | 208.6 | 163.2 | 131.1 | 107.4 |
| | $Z_{0o}(\Omega)$ | 58.45 | 54.21 | 50.14 | 46.24 |
| | $S_C^{-1}(\Omega)$ | 48.56 | 42.63 | 37.49 | 33.02 |
| 20 | $Z_{0e}(\Omega)$ | 257.8 | 201.6 | 162.0 | 132.7 |
| | $Z_{0o}(\Omega)$ | 72.22 | 67.00 | 61.95 | 57.13 |
| | $S_C^{-1}(\Omega)$ | 46.60 | 40.94 | 36.02 | 31.74 |

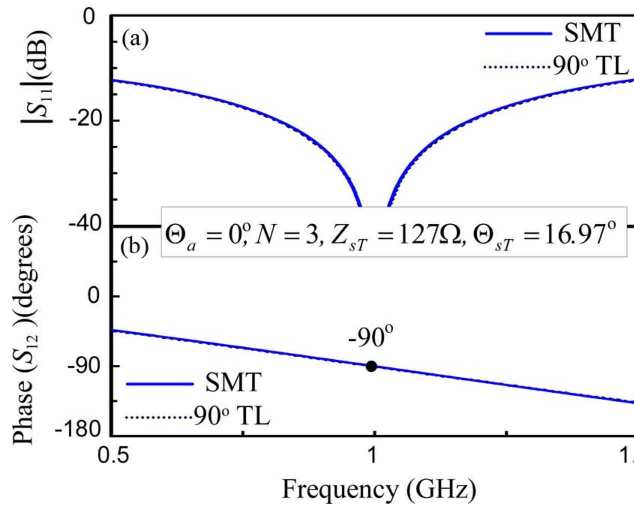


Fig. 10. Frequency responses of one SMT with total length of 51° and a quarter-wave impedance transformer. (a) $|S_{11}|$. (b) Phases of $S_{12}$.

The next is to design three identical 90° transmission-line sections with the characteristic impedance of 70.71 Ω. For a single transmission-line section, either SMT or SMΠ may be possible. For SMT, when $\Theta_a = 0°$ and $N = 3$, if $Z_{sT}$ is chosen as 127 Ω, $\Theta_{sT}$ is then computed as 16.97°. The corresponding susceptance $S_T$ in Fig. 6(b) is $205^{-1}$ ℧, which may be equivalent to 0.7765 pF at a center frequency of 1 GHz. The frequency responses of the 70.71 Ω-SMT mentioned above are compared with those of a 90° transmission-line section (impedance transformer) in Fig. 10 where the solid and dotted lines are those of the SMT and the 90° impedance transformer. Two types of responses in Fig. 10 are identical to each other. If the size is reduced, frequency performance is generally degraded, as demonstrated in Fig. 3 and in the conventional methods [22]–[27]. However, the cases with the SMTs are different. Even though the SMT is 51° long, the performance is about the same as that of the 90° single transmission-line section, which is a big advantage over other conventional equivalent circuits. The reason why the bandwidth of the SMT is the same as that of the 90° transmission-line section is that the scattering parameter of $S_{22}$ of the SMT draws about the same circle of the 90° impedance transformer, just like SMΠ with $N = 3$ demonstrated in Fig. 8.

The coupled-line ring hybrid consisting of three SMTs and one SCΠ is depicted in Fig. 11(a) where the SMT in Fig. 10 is utilized for 90° phase shift, and the SMC is for 270° phase

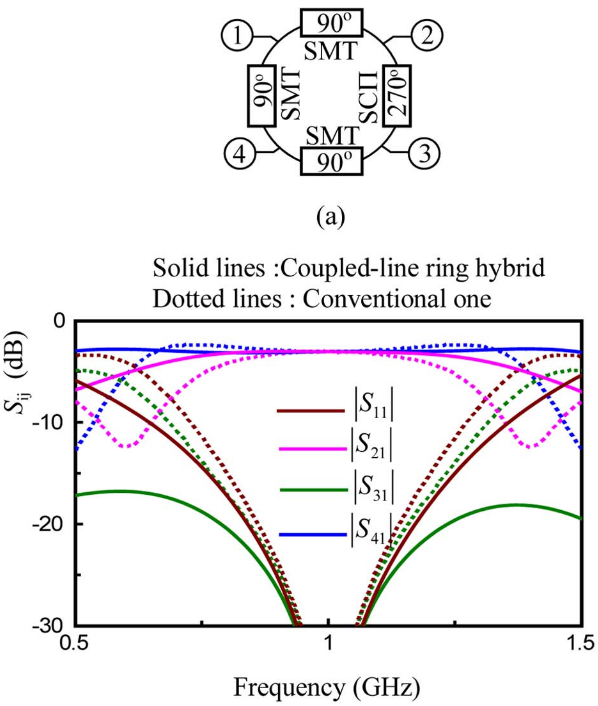


Fig. 11. Coupled-line ring hybrid and its frequency responses. (a) Schematic description of the coupled-line ring hybrid with three SMTs and one SCΠ. (b) Comparisons between the coupled-line ring hybrid with total length of 190° and the conventional one with 540° long.

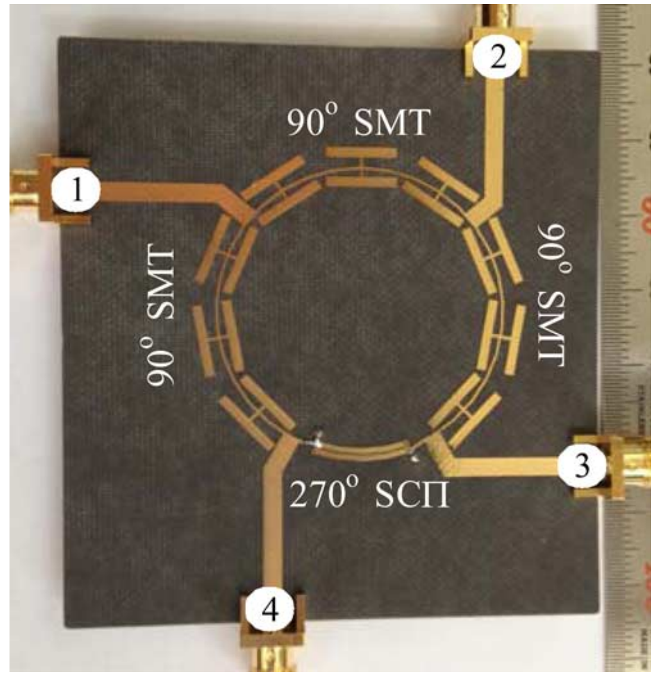


Fig. 12. Photograph of the fabricated coupled-line ring hybrid.

TABLE VI
FABRICATION DATA FOR THE COUPLED-LINE RING HYBRID

| SMT ($N = 3$, $\Theta_a = 0°$) | | | |
|---|---|---|---|
| $Z_{sT}$ | $\Theta_{sT}$ | ${S_T}^{-1}$ | |
| 127 Ω | 16.97° | 205 Ω | |
| SCΠ | | | |
| $Z_a$ | $\Theta_a$ | $\Theta_{sC}$ | ${S_C}^{-1}$ |
| 120 Ω | 5° | 20° | 30.57 Ω |
| $C$ = -8.3 dB | | | |
| $Z_{0e}$ = 125.39 Ω<br>$Z_{0o}$ = 55.73 Ω | | $w$ = 0.7548 mm<br>$s$ = 0.1704 mm | |

shift. The SCΠ for the simulations is the one with $\Theta_{sC} = 27°$ and $C = -7$ dB in Table V, which can be realized in microstrip technology without any difficulty. The frequency responses of the coupled-line ring hybrid are compared with those of the conventional one in Fig. 11(b) where solid and dotted lines are those of the coupled-line and conventional ring hybrids, respectively. The total transmission-line length of the coupled-line ring hybrid is 190°, which is much less than that of the conventional one (540°). Nevertheless, all the scattering parameters of the coupled-line ring hybrid are much better than those of the conventional one, and the isolation performance is far more excellent.

## B. Ring-Hybrid Measurements

To verify the suggested theory, a coupled-line ring hybrid designed at 1 GHz was fabricated on a substrate (RT/Duroid 5880, $\varepsilon_r = 2.2$, $H = 0.787$ mm). The fabricated ring hybrid, consisting of three SMTs and one SCΠ, is displayed in Fig. 12. The SMT is the same as those exemplified in Figs. 10 and 11, and the data of SCΠ are $Z_a = 120\ \Omega$, $\Theta_a = 5°$, $\Theta_{sC} = 20°$, coupling coefficient of $C = -8.3$ dB in Fig. 6(a). The corresponding even- and odd-mode impedances are $Z_{0e} = 125.39$ and $Z_{0e} = 55.73\ \Omega$ for which the line width $w$ and the gap distance of $s$ on the substrate are $w = 0.75$ and $s = 0.17$ mm. All the necessary data for the fabrication are collected in Table VI.

The suceptance of $S_C$ or $S_T$ in (11) and (12) may be realized with one transmission-line section with the characteristic impedance of $Z_{d1}$ and the electrical length of $\Theta_{d1}$ and one lumped capacitor with the capacitance of $C_{SU}$ in Fig. 13(a), or two transmission-line sections with the characteristic impedances of $Z_{d1}$ and $Z_{d2}$ and the electrical lengths of $\Theta_{d1}$ and $\Theta_{d2}$, as illustrated in Fig. 13(b) using the following relations:

$$S_C = Y_{d1} \frac{\omega C_{SU} + Y_{d1} \tan \Theta_{d1}}{Y_{d1} - \omega C_{SU} \tan \Theta_{d1}} \tag{15a}$$

$$S_T = Y_{d1} \frac{Y_{d2} \tan \Theta_{d2} + Y_{d1} \tan \Theta_{d1}}{Y_{d1} - Y_{d2} \tan \Theta_{d1} \tan \Theta_{d2}} \tag{15b}$$

where $\omega$ is the angular frequency at a design center frequency, $Y_{d1} = Z_{d1}^{-1}$ and $Y_{d2} = Z_{d2}^{-1}$.

Based on (15), $Z_{d1} = 120\ \Omega$ and $C_{SU} = 5$ pF at 1 GHz in Fig. 13(a) are calculated for $S_C$. Two 5-pF capacitors (Murata, GRM1885C1H5R0CZ01) are soldered to complete the SCΠ in Fig. 12. $Z_{d1} = 120\ \Omega$, $\Theta_{d1} = 1.95°$, $Z_{d2} = 18\ \Omega$, and $\Theta_{d2} = 2.2°$ in Fig. 13(b) are computed for $S_T/2$.

The measured responses are compared with the predicted ones in Fig. 14 where solid lines and symbols are simulated and measured responses, isolation, and matching are in Fig. 14(a), power divisions in Fig. 14(b), and phase responses in Fig. 14(c). The measured matching, isolation, and power divisions are

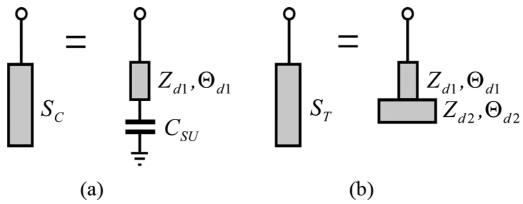


Fig. 13. Susceptance realization with two different ways. (a) One transmission-line section and one lumped capacitor. (b) Two different transmission-line sections.

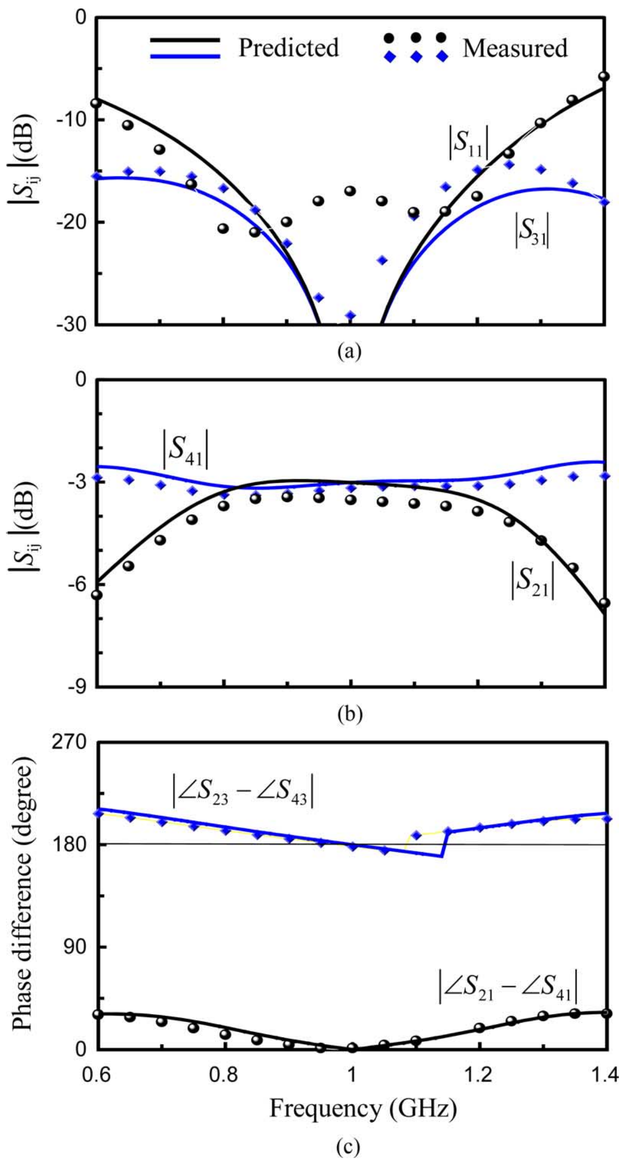


Fig. 14. Measured results of the coupled-line ring hybrid. (a) Matching of $|S_{11}|$ and isolation of $|S_{31}|$. (b) Power divisions of $|S_{21}|$ and $|S_{41}|$. (c) Phase difference between $|S_{23}|$ and $|S_{43}|$ or between $|S_{21}|$ and $|S_{41}|$.

$-17.16$, $-29.88$, $-3.188$, and $-3.442$ dB at 1 GHz. The bandwidth with 15-dB return loss is 50% (0.73–1.23 GHz) and the isolation is better than 14.7 dB in whole frequencies of interest. Good in-phase and out-of-phase responses in Fig. 14(c) are also obtained.

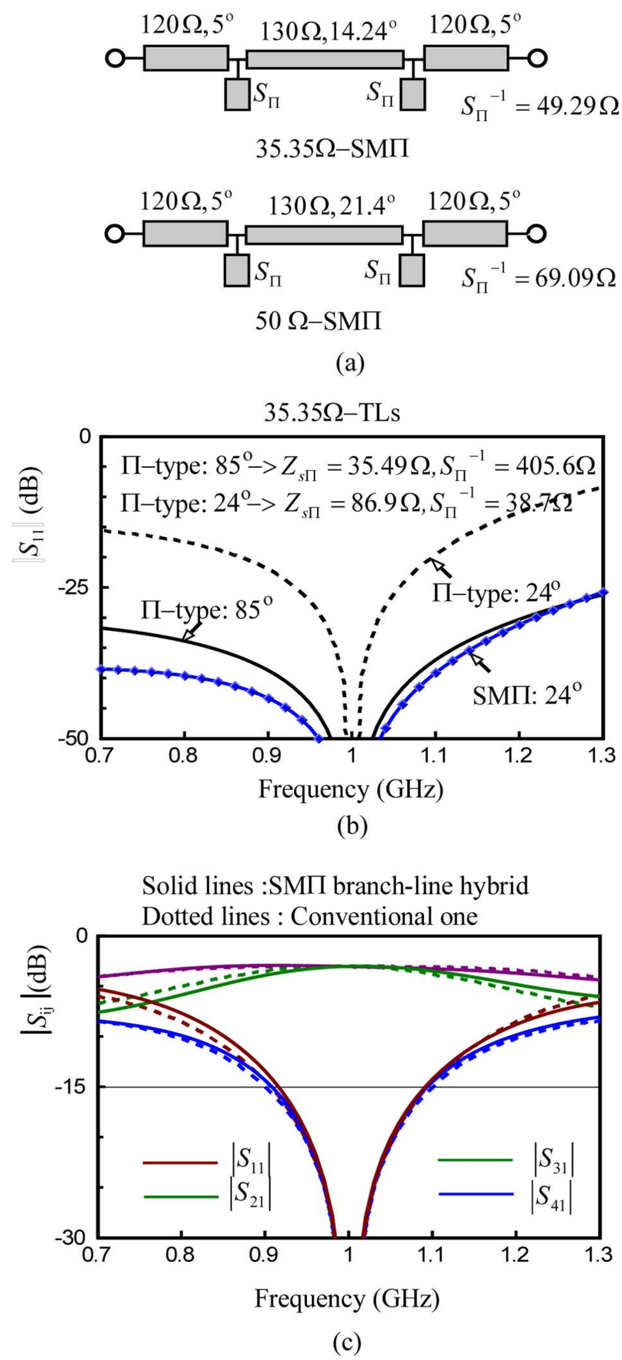


Fig. 15. SMΠs and frequency responses. (a) SMΠs with $N = 1, Z_a = 120\ \Omega$, and $\Theta_a = 5°$. (b) Comparisons between $35.35\ \Omega-$SMΠ and conventional two Π-types. (c) Comparisons between SMΠ branch-line hybrid and conventional one with four 90° transmission-line sections.

## V. Compact Branch-Line Hybrids

### A. Branch-Line Hybrid

The branch-line hybrid has four 90° transmission-line sections and the characteristic impedances of two pairs of the transmission-line sections are 35.35 Ω and 50 Ω. For the size reduction, SMΠs are employed. For both characteristic impedances of 35.35 and 50 Ω, if $Z_a = 120\ \Omega$, $\Theta_a = 5°$, $N = 1$, and $Z_{s\Pi} = 130\ \Omega$ are predetermined, the electrical lengths of $\Theta_{s\Pi}$

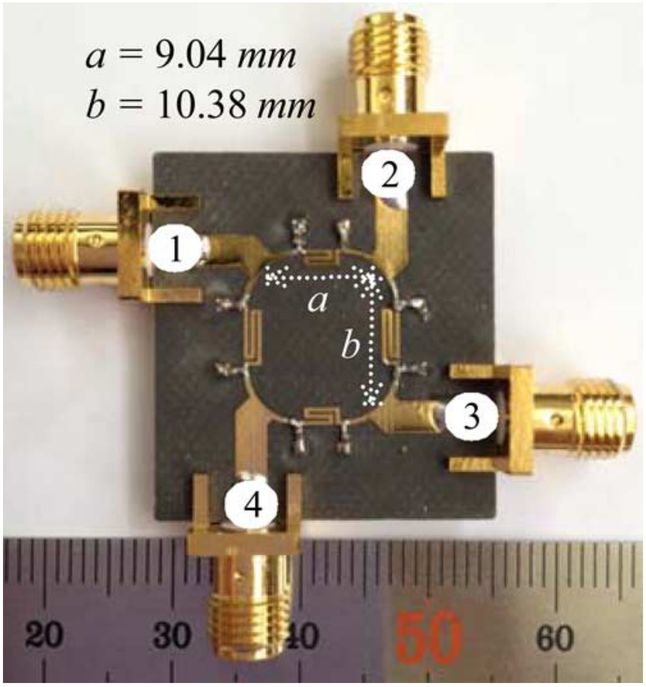


Fig. 16. Photograph of the fabricated branch-line hybrid.

in Fig. 6(c) are calculated as 14.24° and 21.4°, and the susceptances of $S_\Pi$ are computed as $49.29^{-1}$ and $69.1^{-1}$ ℧ for 35.35 and 50 Ω transmission-line sections, respectively, as indicated in Fig. 15(a).

As demonstrated in Fig. 8, to have the ideal performance of the compact branch-line hybrid, $N \geq 2$ is desired, but $N = 1$ was chosen intentionally. The 35.35Ω-SMΠ with the total transmission-line length of 24° at 1 GHz is compared with two conventional Π-types in Fig. 15(b) where the design data of the conventional Π-types are specified, and the frequency response of SMΠ is expressed as solid line with symbols. The bandwidth of the Π-type: 24° is much smaller than that of SMΠ even with the same total lengths, while SMΠ has larger bandwidth than the Π-type: 85° in a frequency range of interest, even though SMΠ is much less than one-third of the Π-type: 85°. The fact demonstrated in Fig. 15(b) validates once more that the equivalent circuits suggested in this paper have definite advantages over the conventional ones. Since SMΠ in Fig. 15(a) may be explained just like two identical MCVTs in Fig. 4(d) are connected in the way that one MCVT is a mirror image of another, the structure itself is symmetric, but its frequency response in Fig. 15(b) is, with respect to the center frequency, more asymmetric than the conventional ones. Therefore, SMΠs discussed so far have the advantage of wider bandwidths with smaller lengths that the asymmetric structures possess inherently, as illustrated in Fig. 5.

Replacing the susceptances of $S_\Pi$ with ideal capacitance values at 1 GHz, the SMΠ branch-line hybrid is compared with the conventional one with four 90° transmission-line sections, and the comparisons are in Fig. 15(c) where the solid and dotted lines are the frequency responses of the SMΠ and conventional branch-line hybrids, respectively. Considering the 15-dB return loss, the bandwidth of the SMΠ branch-line hybrid is just slightly smaller than that of the conventional, even though the total length of SMΠs $(111^\circ)$ is much less than that of the conventional one $(360^\circ)$.

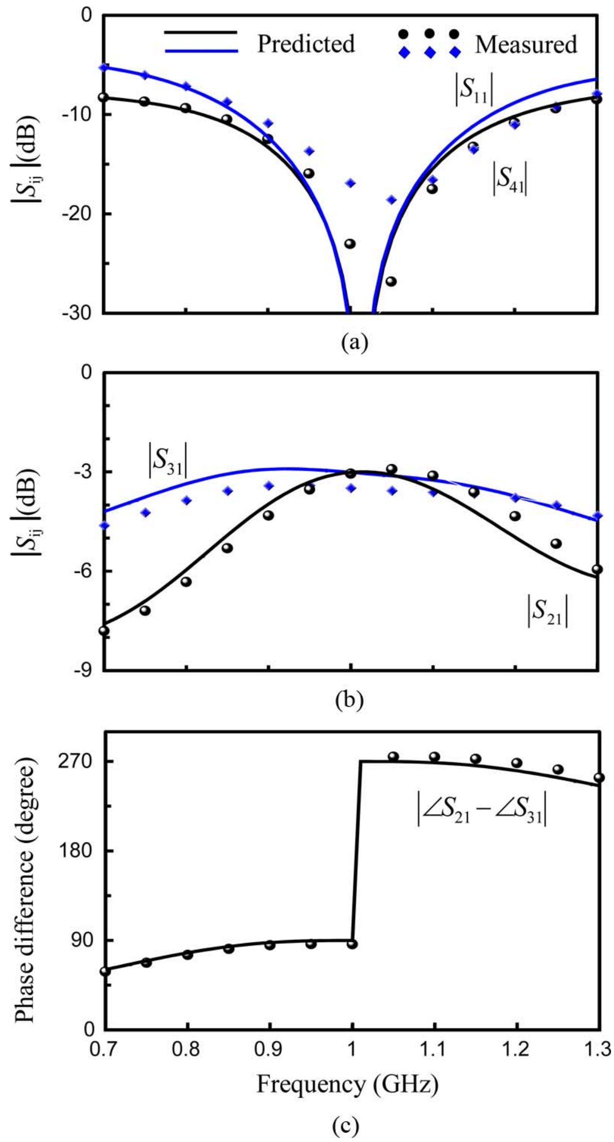


Fig. 17. Measured results of branch-line hybrid. (a) Matching of $|S_{11}|$ and isolation of $|S_{41}|$. (b) Power divisions of $|S_{21}|$ and $|S_{31}|$. (c) Phase difference between $|S_{21}|$ and $|S_{31}|$.

### B. Branch-Line Hybrid Measurements

Based on the data in Fig. 15(a), one compact branch-line hybrid designed at 1 GHz was fabricated on the substrate (RT/Duroid 5880, $\varepsilon_r = 2.2$, $H = 0.787$ mm) and the fabricated branch-line hybrid is displayed in Fig. 16 where the occupied size is 9.04 by 10.38 mm. Each susceptance of $S_\Pi$ was realized with a transmission-line section with the characteristic impedance of 120 Ω and a lumped capacitor, as suggested in Fig. 13(a). The reason for the use of the transmission-line section in Fig. 13(a) is to use available capacitors because the capacitance values provided by the manufacturers are restricted. Obtainable capacitors with 2.2 and 3 pF were soldered, and both are GRM1885C1H series (Murata). The 130-Ω transmission-line sections shown in Fig. 15(a) were meandered for more size reduction, with sufficient gap size between transmission-line sections to avoid couplings.

The measured responses are compared with the predicted ones in Fig. 17 where matching and isolation responses are in Fig. 17(a), power divisions in Fig. 17(b), and phase difference between $S_{21}$ and $S_{31}$ in Fig. 17(c). The measured matching, isolation, and power divisions at 1 GHz are $-16.9$, $-25.29$, $-3.02$, and $-3.484$ dB and good phase response is also obtained.

## VI. Conclusions

New types of symmetric equivalent circuits were suggested to reduce the size of ring and branch-line hybrids with more design flexibility, easier fabrication with 2-D structures, and better frequency performance. To introduce the equivalent circuits, the SITL sections were first synthesized and new equivalent circuits were derived by combining the SITL sections and coupled-line $\Pi$-type, modified $\Pi$-, or $T$-type. To distinguish, they were called SC$\Pi$, SM$\Pi$, and SMT, and one coupled-line ring hybrid and one branch-line hybrid were implemented based on these equivalent circuits. The ring hybrid consisted of three SMTs and one SC$\Pi$, while the branch-line hybrid was made of two sets of SM$\Pi$s, and the resulting total lengths of transmission-line sections are 183° and 111°, respectively. The fabricated ring and branch-line hybrids may be considered as good results, considering size and frequency performances, and the suggested equivalent circuits may be employed for diverse applications, requiring compactness.

## References


[1] H.-R. Ahn and I. Wolff, “Asymmetric four-port and branch-line hybrids,” *IEEE IEEE Trans. Microw. Theory Techn.*, vol. 48, no. 9, pp. 1585–1588, Sep. 2000.

[2] H.-R. Ahn, I. Wolff, and I.-S. Chang, “Arbitrary termination impedances, arbitrary power division, and small-sized ring hybrids,” *IEEE IEEE Trans. Microw. Theory Techn.*, vol. 45, no. 12, pp. 2241–2247, Dec. 1997.

[3] H.-R. Ahn, I.-S. Chang, and S.-W. Yun, “Miniaturized 3-dB ring hybrid terminated by arbitrary impedances,” *IEEE IEEE Trans. Microw. Theory Techn.*, vol. 42, no. 12, pp. 2216–2221, Dec. 1994.

[4] H.-R. Ahn and T. Itoh, “New isolation circuits of compact impedance-transforming 3-dB baluns for theoretically perfect isolation and matching,” *IEEE Trans. Microw. Theory Techn.*, vol. 58, no. 12, pp. 3892–3902, Dec. 2010.

[5] H.-R. Ahn and B. Kim, “Small wideband coupled-line ring hybrids with no restriction on coupling power,” *IEEE Trans. Microw. Theory Techn.*, vol. 57, no. 7, pp. 1806–1817, Jul. 2009.

[6] M. K. Mandal and S. Sanyal, “Reduced-length rat-race couplers,” *IEEE IEEE Trans. Microw. Theory Techn.*, vol. 55, no. 12, pp. 2593–2598, Dec. 2007.

[7] H. Ghali and T. A. Moselhy, “Miniaturized fractal rat-race, branch-line, and coupled-line hybrids,” *IEEE Trans. Microw. Theory Techn.*, vol. 52, no. 11, pp. 2513–2520, Nov. 2004.

[8] S.-S. Liao, P.-T. Sun, N.-C. Chin, and J.-T. Peng, “A novel compact-size branch-line coupler,” *IEEE Microw. Wireless Compon. Lett.*, vol. 15, no. 9, pp. 588–590, Sep. 2005.

[9] S.-S. Liao and J.-T. Peng, “Compact planar microstrip branch-line couplers using the quasi-lumped elements approach with nonsymmetrical and symmetrical T-shaped structure,” *IEEE Trans. Microw. Theory Techn.*, vol. 54, no. 9, pp. 3508–3514, Sep. 2006.

[10] V. K. Velidi, S. Shrivastava, and S. Sanyal, “Improved compact spurious passband suppression rat-race coupler using asymmetric T-shaped units,” *Microw. Opt. Technol. Lett.*, vol. 53, pp. 2248–2251, Oct. 2011.

[11] C.-H. Tseng and C.-L. Chang, “A rigorous design methodology for compact planar branch-line and rat-race couplers with asymmetrical T-structures,” *IEEE IEEE Trans. Microw. Theory Techn.*, vol. 60, no. 7, pp. 2085–2092, Jul. 2012.

[12] H.-R. Ahn and I. Wofff, “General design equations, small-sized impedance transformers, and their applications to small-sized three-port 3-dB power dividers,” *IEEE Trans. Microw. Theory Techn.*, vol. 49, no. 7, pp. 1277–1288, Jul. 2001.

[13] H.-R. Ahn and T. Itoh, “Compact impedance-transforming 3-dB three-port power dividers with modified asymmetric impedance transformers (MCCTS),” in *IEEE MTT-S Int. Microw. Symp. Dig.*, Baltimore, MD, USA, Jun. 2011, Art. ID TH1B-2.

[14] H.-R. Ahn, “Modified asymmetric impedance transformers (MCCTs and MCVTs) and their application to impedance-transforming three-port 3-dB power dividers,” *IEEE Trans. Microw. Theory Techn.*, vol. 59, no. 12, pp. 3312–3321, Dec. 2011.

[15] H.-R. Ahn and B. Kim, “Modified small asymmetric impedance transformers,” in *IEEE MTT-S Int. Microw. Symp. “Art of Miniaturizing RF and Microwave Passive Components” Workshop*, 2008, pp. 71–74.

[16] T.-N. Kuo, Y.-S. Lin, C.-H. Wang, and C. H. Chen, “A compact LTCC branch-line coupler using modified-T equivalent-circuit model for transmission line,” *IEEE Microw. Wireless Compon. Lett.*, vol. 16, no. 2, pp. 90–92, Feb. 2006.

[17] K.-O. Sun, S.-J. Ho, C.-C. Yen, and D. Weide, “A compact branch-line coupler using discontinuous microstrip lines,” *IEEE Microw. Wireless Compon. Lett.*, vol. 15, no. 8, pp. 519–520, Aug. 2005.

[18] R. W. Vogel, “Analysis and design of lumped- and lumped-distributed element directional couplers for MIC and MMIC applications,” *IEEE Trans. Microw. Theory Techn.*, vol. 40, no. 2, pp. 253–262, Feb. 1992.

[19] H. Okabe, C. Caloz, and T. Itoh, “A compact enhanced-bandwidth hybrid ring using an artificial lumped-element left-handed transmission-line section,” *IEEE Trans. Microw. Theory Techn.*, vol. 52, no. 3, pp. 798–804, Mar. 2004.

[20] G. Monti and L. Tarricone, “Compact broadband monolithic 3-dB coupler by using artificial transmission lines,” *Microw. Opt. Technol. Lett.*, vol. 50, no. 10, pp. 2662–2667, Oct. 2008.

[21] H.-S. Lee, K. Choi, and H.-Y. Hwang, “A harmonic and size reduced ring hybrid using coupled lines,” *IEEE Microw. Wireless Compon. Lett.*, vol. 17, no. 4, pp. 259–261, Apr. 2007.

[22] D. Nesic, “Slow-wave EBG microstrip rat-race hybrid ring,” *Electron. Lett.*, vol. 41, pp. 1181–1183, Oct. 2005.

[23] J. Wang, B.-Z. Wang, Y.-X. Guo, L. C. Ong, and S. Xiao, “Compact slow-wave microstrip rat-race ring coupler,” *Electron. Lett.*, vol. 43, pp. 111–113, Feb. 2007.

[24] J. Wang, B. Z. Wang, Y.-X. Guo, L.-C. Ong, and S. Xiao, “A compact slow-wave microstrip branch-line coupler with high performance,” *IEEE Microw. Wireless Compon. Lett.*, vol. 17, no. 7, pp. 501–503, Jul. 2007.

[25] C.-W. Tang and M.-G. Chen, “Synthesizing microstrip branch-line couplers with predetermined compact size and bandwidth,” *IEEE Trans. Microw. Theory Techn.*, vol. 55, no. 9, pp. 1926–1934, Sep. 2007.

[26] H.-X. Xu, G.-M. Wang, and K. Lu, “Microstrip rat-race couplers,” *IEEE Microw. Mag.*, vol. 12, no. 4, pp. 117–129, Apr. 2011.

[27] C.-H. Tseng and H.-J. Chen, “Compact rat-race coupler using shunt-stub-based artificial transmission lines,” *IEEE Microw. Wireless Compon. Lett.*, vol. 18, no. 11, pp. 734–736, Nov. 2008.

[28] H.-R. Ahn and S. Nam, “New design formulas for impedance-transforming 3-dB Marchand baluns,” *IEEE Trans. Microw. Theory Techn.*, vol. 59, no. 11, pp. 2816–2823, Nov. 2011.

[29] K. W. Eccleston and S. H. M. Ong, “Compact planar microstripline branch-line and rat-race coupler,” *IEEE Trans. Microw. Theory Techn.*, vol. 51, no. 10, pp. 2119–2125, Oct. 2003.

[30] S.-S. Liao, J.-T. Peng, and C.-Y. Gun, “A super compact planar microstripline rat-race coupler,” *Microw. Opt. Technol. Lett.*, vol. 47, pp. 302–304, Nov. 2005.

[31] J.-T. Kuo, J.-S. Wu, and Y.-C. Chiou, “Miniaturized rat race coupler with suppression of spurious passband,” *IEEE Microw. Wireless Compon. Lett.*, vol. 17, no. 1, pp. 46–48, Jan. 2007.

[32] M.-L. Chuang, “Miniaturized ring coupler of arbitrary reduced size,” *IEEE Microw. Wireless Compon. Lett.*, vol. 15, pp. 16–18, Jan. 2005.

[33] T. Hirota, A. Minakawa, and M. Muraguchi, “Reduced-size branch-line and rat-race hybrids for uniplanar MMIC’s,” *IEEE Trans. Microw. Theory Techn.*, vol. 38, no. 3, pp. 270–275, Mar. 1990.

[34] J. Gu and X. Sun, “Miniaturization and harmonic suppression of branch-line and rat-race hybrid coupler using compensated spiral compact microstrip resonant cell,” in *IEEE MTT-S Int. Microw. Symp. Dig.*, 2005, pp. 1211–1214.

[35] V. K. Velidi, D. K. Pandey, and S. Sanyal, “Microstrip rat-race couplers with predetermined miniaturization and harmonic suppression,” *Microw. Opt. Technol. Lett.*, vol. 52, pp. 30–34, Jan. 2010.

[36] W. Shao, J. He, and B.-Z. Wang, “Compact rat-race ring coupler with capacitor loading,” *Microw. Opt. Technol. Lett.*, vol. 52, pp. 7–9, Jan. 2010.

[37] Q.-X. Chu and F. Lin, “A novel tri-band rat-race coupler with T-shaped step impedance transformers,” *Microw. Opt. Technol. Lett.*, vol. 52, pp. 1240–1244, Jun. 2010.

[38] S. Opozda, P. Kurgan, and M. Kitlinski, “A compact seven-section rat-race hybrid coupler incorporating PBG cells,” *Microw. Opt. Technol. Lett.*, vol. 51, pp. 2910–2913, Dec. 2009.

[39] C.-W. Tang, M.-G. Chen, and C.-H. Tsai, “Miniaturization of microstrip branch-Line coupler with dual transmission lines,” *IEEE Microw. Wireless Compon. Lett.*, vol. 18, no. 3, pp. 185–187, Mar. 2008.

[40] M. Ali, S. K. A. Rahim, M. Z. M. Nor, and M. F. Jamlos, “Branch line coupler using hybrid T-model structure,” *Microw. Opt. Technol. Lett.*, vol. 54, pp. 237–240, Jan. 2012.

[41] Y.-H. Chun and J.-S. Hong, “Compact wide-band branch-line hybrids,” *IEEE Trans. Microw. Theory Techn.*, vol. 54, no. 2, pp. 704–709, Feb. 2006.

[42] M. K. Mandal, V. K. Velidi, A. Bhattacharya, and S. Sanya, “Miniaturized quadrature hybrid coupler using high impedance lines,” *Microw. Opt. Technol. Lett.*, vol. 50, pp. 1135–1137, May 2008.

[43] K.-Y. Tsai, H.-S. Yang, J.-H. Chen, and Y.-J. E. Chen, “A miniaturized 3 dB branch-line hybrid coupler with harmonics suppression,” *IEEE Microw. Wireless Compon. Lett.*, vol. 21, pp. 537–539, Oct. 2011.

[44] S. C. Jung, R. Negra, and F. M. Ghannouchi, “A design methodology for miniaturized 3-dB branch-line hybrid couplers using distributed capacitors printed in the inner area,” *IEEE Trans. Microw. Theory Techn.*, vol. 56, no. 12, pp. 2950–2953, Dec. 2008.

[45] C.-L. Hsu, J.-T. Kuo, and C.-W. Chang, “Miniaturized dual-band hybrid couplers with arbitrary power division ratios,” *IEEE Trans. Microw. Theory Techn.*, vol. 57, no. 1, pp. 149–156, Jan. 2009.

[46] K. Hettak, G. A. Morin, and M. G. Stubbs, “Compact MMIC CPW and asymmetric CPS branch-line couplers and wilkinson dividers using shunt and series stub loading,” *IEEE Trans. Microw. Theory Techn.*, vol. 53, no. 5, pp. 1624–1635, May 2005.

[47] H.-R. Ahn, *Asymmetric Passive Components in Microwave Integrated Circuits*. New York: Wiley, 2006, pp. 32–32.

[48] H. R. Ahn and B. Kim, “Toward integrated circuit size reduction,” *IEEE Microw. Mag.*, vol. 9, no. 1, pp. 65–75, Feb. 2008.

[49] D. A. Frickey, “Conversions between $S$, $Z$, $Y$, $H$, $ABCD$, and $T$ parameters which are valid for complex source and load impedances,” *IEEE Trans. Microw. Theory Techn.*, vol. 42, no. 2, pp. 205–211, Feb. 1994.


**Hee-Ran Ahn** (S’90–M’95–SM’99) received the B.S., M.S., and Ph.D. degrees in electronic engineering from Sogang University, Seoul, Korea, in 1988, 1990, and 1994, respectively.

Since April 2011, she has been with the School of Electrical Engineering and Computer Science, Seoul National University, Seoul Korea. From August 2009 to December 2010, she was with the Department of Electrical Engineering, University of California at Los Angeles, Los Angeles, CA, USA. From July 2005 to August 2009, she with the Department of Electronics and Electrical Engineering, Pohang University of Science and Technology, Pohang, Korea. From 2003 to 2005, she with the Department of Electrical Engineering and Computer Science, Korea Advanced Institute of Science and Technology, Daejeon, Korea. From 1996 to 2002, she was with the Department of Electrical Engineering, Duisburg–Essen University, Duisburg, Germany, where she was involved with the Habilitation dealing with asymmetric passive components in microwave circuits. She authored *Asymmetric Passive Component in Microwave Integrated Circuits* (Wiley, 2006). Her interests include high-frequency and microwave circuit designs and biomedical applications using microwave theory and techniques.

**Sangwook Nam** (S’87–M’88–SM’11) received the B.S. degree from Seoul National University, Seoul, Korea, in 1981, the M.S. degree from the Korea Advanced Institute of Science and Technology (KAIST), Seoul, Korea, in 1983, and the Ph.D. degree from The University of Texas at Austin, Austin, TX, USA, in 1989, all in electrical engineering.

From 1983 to 1986, he was a Researcher with the Gold Star Central Research Laboratory, Seoul, Korea. Since 1990, he has been a Professor with the School of Electrical Engineering and Computer Science, Seoul National University. His research interests include analysis/design of electromagnetic (EM) structures and antennas and microwave active/passive circuits.